Neoplasia • Vol. 6, No. 3, May/June 2004, pp. 224–233 224

www.neoplasia.com

Photodynamic Therapy of Established Prostatic Adenocarcinoma with TOOKAD: A Biphasic Apparent Diffusion Coefficient Change as Potential Early MRI Response Marker[1]

Vicki Plaks, Natalia Koudinova*, Uri Nevo[†,‡], Jehonathan H. Pinthus[§,¶], Hannah Kanety[#], Zelig Eshhar[§], Jacob Ramon[¶], Avigdor Scherz**, Michal Neeman* and Yoram Salomon**

Departments of *Biological Regulation and [†]Neurobiology, The Weizmann Institute of Science, Rehovot 76100, Israel; [‡]Tel-Aviv University, School of Physics and Astronomy, Tel-Aviv 69978, Israel; [§]Department of Immunology, The Weizmann Institute of Science, Rehovot 76100, Israel; Departments of [¶]Urology and [#]The Institute of Endocrinology, Sheba Medical Center, Tel Hashomer 52621, Israel; **Department of Plant Sciences, The Weizmann Institute of Science, Rehovot 76100, Israel

Abstract

The goal of this study was to examine the use of diffusion-weighted magnetic resonance imaging (DW-MRI) for the assessment of early progression of photodamage induced by Pd-bacteriopheophorbide (TOOKAD)–based photodynamic therapy (PDT). TOOKAD is a novel second-generation photosensitizer for PDT of solid tumors developed in our laboratory and presently under clinical trials for prostate cancer (PC) therapy. Using the subcutaneous human prostate adenocarcinoma WISH-PC14 xenografts in nude mice as a model, a unique biphasic change in the apparent diffusion coefficient (ADC) was observed within the first 24 hours post-PDT, with initial decrease followed by an increase in ADC. Using DW-MRI, this phenomenon enables the detection of successful tumor response to PDT within 7 hours posttreatment. This process was validated by direct, histological, and immunohistochemical examinations and also by evaluation of serum prostate-specific antigen (PSA) levels that decreased significantly already 7 hours posttreatment. *In vitro* studies of multicellular cell spheroids confirmed a PDT-induced decrease in ADC, suggesting that lipid peroxidation (LPO) significantly contributes to ADC decline observed after PDT. These results demonstrate that TOOKAD-based PDT successfully eradicates prostate adenocarcinoma xenografts and suggests DW-MRI to be useful for the detection of early tumor response and treatment outcome in the clinical setting.

Neoplasia (2004) **6**, 224–233

Keywords: Diffusion MRI, photodynamic therapy, human prostate adenocarcinoma, TOOKAD, cell spheroid.

Introduction

Photodynamic therapy (PDT) of tumors [1] with Pd-bacteriopheophorbide (TOOKAD) [2,3] relies on *in situ* photosensitization of the circulating sensitizer with consequent generation of cytotoxic reactive oxygen species (ROS) [4]. Local ROS generation in the treated tumor induces rapid vascular occlusion and hypoxia and initiates lipid peroxidation (LPO) primarily in the tumor vasculature, spreading throughout the tumor within hours after treatment [5–8]. Overall cytotoxicity of PDT results in cell death and necrosis of tumor components with minimal damage to the surrounding tissues [9,10]. We previously demonstrated that this treatment modality induces significant cure rates of different xenograft models in mice [3,5–7,11] and in rats [12]. Prostate cancer (PC) is the most commonly diagnosed noncutaneous malignancy and is the second leading cause of cancer-related death in American men [13]. Moreover, PC is the cause of substantial morbidity and serious complications from both local tumor and distant metastases.

We previously showed that TOOKAD-PDT is a feasible, efficient, and well-tolerated approach for minimally invasive treatment of local and disseminated human small cell carcinoma of the prostate (SCCP) and bone lesions model in mice [6]. Furthermore, TOOKAD-PDT was recently suggested as an alternative for PC treatment as it induces lesions in a canine prostate model, with no evidence of urinary side effects or nearby tissue damage [14]. Phase I/II clinical trials of TOOKAD-PDT on patients with recurrent PC following failed

Abbreviations: ADC, apparent diffusion coefficient; DW, diffusion-weighted; MRI, magnetic resonance imaging; ECS, extracellular space; HNE, 4-hydroxy-2-nonenal; LPO, lipid peroxidation; PC, prostate cancer; PDT, photodynamic therapy; ROS, reactive oxygen species; WISH-PC14, Weizmann Institute Sheba Hospital prostate cancer 14; SCCP, small cell carcinoma of the prostate; PI, propidium iodide; ROI, region of interest

Address all correspondence to: Prof. Yoram Salomon, Department of Biological Regulation, The Weizmann Institute of Science, Rehovot 76100, Israel.
E-mail: yoram.salomon@weizmann.ac.il

[1]This study is in partial fulfillment of the MSc thesis of V.P. for the Feinberg Graduate School, The Weizmann Institute of Science. Y.S. is the incumbent of the Tillie and Charles Lubin Professorial Chair in Biochemical Endocrinology. A.S. is the incumbent of the Robert and Yadele Sklare Professional Chair in Biochemistry. This study was supported, in part, by the Wilner Foundation for Vascular Biology and by STEBA BIOTECH (Toussus-Le-Noble, France).
Received 23 September 2003; Revised 2 December 2003; Accepted 3 December 2003.

Copyright © 2004 Neoplasia Press, Inc. All rights reserved 1522-8002/04/$25.00
DOI 10.1593/neo.03352

external beam radiation therapy are presently underway in Canada [15].

Tumor response to chemotherapy and radiotherapy is commonly assessed by radiographic changes in tumor morphology or, in the case of PC, often relies on serum levels of prostate-specific antigen (PSA) [13] requiring time elapses of weeks to months posttreatment in both cases. Because TOOKAD-PDT is a single-session treatment modality performed within an hour or so, rapid assessment of response to therapy will be an attractive virtue of this minimally invasive treatment, allowing immediate patient reprognostification and early consideration of adjuvant treatment.

Magnetic resonance can noninvasively provide a wealth of information regarding tumor morphology, metabolism, and pathology, thereby allowing the assessment of the response to treatment by changes induced on these parameters. Several magnetic resonance imaging (MRI) techniques have been employed for the detection of response to therapy in various types of cancer in both clinical and preclinical models. Among the examples are T2-weighted imaging [16], T1-weighted imaging [17], and dynamic contrast-enhanced imaging [11,18]. Displacement of water molecules has become a major intrinsic MRI contrast tool, providing the sharpest discrimination between healthy and malignant (prostatic) tissues [19,20]. As such, diffusion-weighted magnetic resonance imaging (DW-MRI) is also a powerful tool for the assessment of damage induced in tumors by cytotoxic therapies when changes in cell vitality are often associated with significant changes in water diffusion. In preclinical models, DW-MRI was shown to be a reliable tool for the detection of tumor response to chemotherapy, irradiation, and gene therapy, relatively early in the treatment regimen [19]. We therefore examined the possibility to assess treatment response by applying DW-MRI for rapid monitoring of PC response to TOOKAD-PDT. Although the exact mechanisms underlying changes in apparent diffusion coefficient (ADC) following therapy are unascertained, it is commonly hypothesized that the increased ADC characteristic of cytotoxic response is due to major cell loss, reduced cell density, and widening of the extracellular space (ECS)—all resulting in water liberation [19].

Using DW-MRI following TOOKAD-PDT of human prostate adenocarcinoma xenografts, we demonstrate that response to treatment, similar to other cancer therapies, is characterized by an increase in ADC as soon as 2 days after PDT. However, quite surprisingly, prior to that rise in ADC and as early as 7 hours after PDT, a significant decrease in ADC was observed. In order to examine the role of the nonvascular compartment in early response to TOOKAD-PDT, we used *in vitro* multicellular spheroids as an avascular tumor model [21–23] and also observed a PDT-induced decrease in ADC. To the best of our knowledge, a decline in ADC in response to PDT in tumors has not been previously reported. The results obtained in this study suggest a unique ADC-dependent pattern of tumor response to TOOKAD-PDT that could eventually be useful in early clinical monitoring of response to therapy.

Materials and Methods

Photosensitizer

For animals TOOKAD (2.5 mg/ml) was administered in 5% Cremophor El–based formulation (NEGMA-LERADS, Toussus-Le-Noble, France).

For spheroids TOOKAD was prepared as previously described [24]. Stock solution (1 mM) was prepared with dimethyl sulfoxide (DMSO) and further diluted with culture medium to 10 μM of 1% DMSO.

Tumor Xenograft Studies

Animal and tumor model Cell suspension of human prostate adenocarcinoma (Weizmann Institute Sheba Hospital prostate cancer 14, WISH-PC14) originating from a recurrent tumor of a postdefinitive radiation therapy patient was prepared as described previously [25]. Cells were mixed with Matrigel (1:1, vol/vol) (Becton Dickinson, Bedford, MA) and subcutaneously injected in the hind limb of CD-1 male nude mice (mice weight 28–32 g, 10×10^6 cells/mouse).

All animal experiments were approved by the Weizmann Institute Institutional Animal Care and Use Committee.

PDT protocol for animals PDT was performed on subcutaneous xenografts 7 to 12 mm in diameter (tumor reached treatment size in 4–5 weeks). Mice were anesthesized with intraperitoneal injection of 75 mg/kg Ketaset (ketamine; Fort Dodge Laboratories, Fort Dodge, IA) and 3 mg/kg XYL-M (xylazine; VMD, Arendonk, Belgium) followed by subcutaneous addition of about 30% of the initial dose in order to prolong anesthesia. Anesthesized mice were intravenously injected with 10 mg/kg TOOKAD and the tumor was immediately illuminated for 10 minutes (108 J/cm^2) using a 763-nm, 1-W diode laser (Ceramoptec, Bonn, Germany). The light spot diameter included a 2 to 3 mm margin around the tumor. Tumor response was recorded by DW-MRI and was additionally examined by direct tumor documentation (photography and volume determination), histological techniques, and immunohistochemical techniques. Serum PSA levels were also determined. Tumor volume (mm^3) was determined by caliper measurement using the formula: length × width × depth × 0.5236 [26] and verified by MRI (see below). All therapeutic results were obtained following a single treatment session.

Controls: light control (illumination [108 J/cm^2] only) and dark control (TOOKAD [10 mg/kg] only).

Diffusion MRI of animals Animals were studied in a horizontal 4.7 T Biospec spectrometer (Bruker, Germany) using an actively radiofrequency (RF)–decoupled 1.5 cm surface coil (for RF receiving) and a whole-body transmission coil. Pulsed gradient spin-echo MRI protocol was applied on axial slices before and after PDT. Anesthetized mice were placed in a homebuilt half-cylindrical Perspex cradle that allowed stable positioning of the mouse, such that the tumor was located on top of the surface coil center. Prior to DW-MRI scans, axial and coronal scout images were obtained to

determine position, extent, and size of the tumor. ADC was measured along a single direction, assuming that water diffusion in the tumor is isotropic as in other prostate xenografts in mice [13,20]. DW-MRI scans were performed with a diffusion gradient linearly incremented in the range of 0 to 150 mT/m with Δ = 35 milliseconds; δ = 3 milliseconds, yielding four *b* values: 6.9, 93.9, 290.4, and 596.4 sec/mm^2; time to repetition (TR) = 2000 milliseconds; time to echo (TE) = 47.7 milliseconds, with two average repetitions; matrix dimensions = 128 $\times$ 128; FOV = 3.5 cm; slice thickness = 1 mm; number of slices (covering entire tumor volume) = 5 or 7, depending on tumor size; total time = 34 minutes. Mice were covered with a recirculating water-filled heating pad to maintain core body temperature at 37°C during the course of MRI experiments.

Each animal underwent MRI examination prior to treatment and at indicated time points (7, 24, and 48 hours) posttreatment with further monitoring of tumor elimination (up to 15–30 days) or histological examination of tumor response.

Determination of PSA Serum PSA levels before and at indicated time points after PDT were determined on serum samples using two chemiluminescent immunometric assays (LKPS1 and LKUP1 PSA kits, Immulite; Diagnostic Products Corp., Los Angeles, CA).

Spheroid Model Studies

Spheroid culture Hepa-1 (murine hepatoma-1) [27] spheroids were cultured in Dulbecco's modified Eagle's medium (DMEM) containing 25 mM HEPES, pH 7.4, 10% heat-inactivated fetal calf serum (Biological Industries, Bet Haemek, Israel), glutamine (2 mM), penicillin (0.06 mg/ml), and streptomycin (0.1 mg/ml) to the size of ~1 mm in diameter, as described earlier [27].

PDT protocol for spheroids Spheroids were preincubated for 4 hours in the dark with 10 μM TOOKAD, washed with fresh culture medium to remove unbound sensitizer, and illuminated for 10 minutes at room temperature through the bottom of a culture Petri dish (650 nm < λ >800 nm, 18 J/cm^2). Photocytotoxicity was analyzed by fluorescent staining with propidium iodide (PI) (Sigma Chemical Co., St. Louis, MO). Briefly, spheroids were incubated with 10 μg/ml PI for 30 minutes, washed twice with fresh medium, and visualized by fluorescent microscopy (Optiphot2 fluorescent microscope; Nikon, Tokyo, Japan) equipped with a CCD camera (DVC Inc., Austin, TX). In the PDT group, only PDT- responsive spheroids in which the viable rim was positively stained were scanned by MRI.

Controls: untreated (no light, no TOOKAD); light control (illuminated only, in medium with 1% DMSO); dark control (TOOKAD incubation in the dark [10 μM, 4 hours], without illumination); and PI only (10 μg/ml, 30 minutes).

Diffusion MRI of spheroids Studies were performed on a vertical-bore 9.4 T DMX 400 MHz spectrometer (Bruker) equipped with an actively shielded NMR microscopy unit. Pulsed gradient spin-echo MRI protocol was applied on axial slices of spheroids before and 20 hours after PDT. DW-MRI scans were performed with a diffusion gradient incremented linearly in the range of 0 to 190 mT/m with Δ = 16.7 milliseconds, δ = 6 milliseconds, yielding four *b* values: 182.6, 604.6, 1328.2, and 2353.3 sec/mm^2; TR = 2000 milliseconds; TE = 31.5 milliseconds, with two averaging repetitions; matrix dimensions = 128 $\times$ 128; FOV = 0.5 cm; slice thickness = 0.3 mm; single slice per scan; total time = 34 minutes; and temperature = 37°C.

MRI data analysis

MRI data were analyzed on an Indigo-2 /02 workstation (Silicon Graphics, Mountain View, CA) using Paravision software (Bruker) and MATLAB (The MathWork, Inc., Natik, MA).

The MR signal was fitted to a monoexponential decay: $S / S_0 = \exp[-b^*\text{ADC}]$, where S and S_0 are water signal intensities in the presence and absence of diffusion-sensitizing gradients, respectively, and *b* is the diffusion weighting factor comprised of δ (duration of gradient pulse), Δ (separation of gradient pulses), γ (gyromagnetic ratio), and G (gradient pulse strength), and also includes cross terms between imaging gradients and diffusion-sensitizing gradients [28]. Diffusion maps for each slice were generated, yielding ADC values for each pixel, and further analyzed by means of region-of-interest (ROI) measurements (taken from all slices where tumor is clearly identified) and were assembled to yield the mean ADC of the tumor. ADC histograms of the tumors at indicated time points after PDT were generated from ROIs combined across slices.

As only a single slice can be measured in spheroids, the mean ADC of a number of spheroids in the experimental group was calculated. Mean ADCs of tumor/spheroids at each time point were subjected to two-tailed *t*-test.

Histology

Tumors (harvested from euthanized mice) were fixed and prepared for histological examination as described earlier [6].

Immunohistochemistry

Paraffin-embedded histological sections of tumors/spheroids were immunostained for the presence of PDT-induced LPO product, 4-hydroxy-2-nonenal (HNE), as described earlier [6].

Results

The Response of Human WISH-PC14 Xenografts to TOOKAD-Based PDT

Tumor-bearing mice received either one treatment session of TOOKAD-PDT, TOOKAD alone (dark control), or illumination alone (light control). In PDT-treated tumors, local inflammatory response was observed within hours after treatment, developing into visible necrosis by 24 to 48 hours. Necrosis appeared as a dark crust on the skin by 48 to 72 hours and reached its maximal size by 4 to 6 days. The healing process culminated with complete tissue remodeling

by 15 to 30 days (Figure 1*A*). Out of 19 treated animals, 14 (74%) exhibited complete necrosis (at 48–72 hours) and five exhibited partial or no response. From the responding group, two were sacrificed for histological examination and three died from unknown reasons. The remaining nine mice were followed up to complete recovery for 30 days. Dark (n = 4) and light (n = 4) (Figure 1*B*) controls were unaffected and continued to grow. The mice were euthanized 15 to 30 days posttreatment to avoid excessive tumor burden ($\geq$ 2000 mm^3).

In a separate experiment, tumor response to PDT was also evaluated by examination of serum PSA (Figure 1*C*). A significant 50% decrease in PSA was detected already 7 hours after PDT, which continued to decline, reaching undetectable levels (< 1%) by 1 week after treatment. In the light control (LC), PSA levels continued to increase rapidly. Initial PSA level of all xenografts tested (n = 13) was 15 ± 12 SD ng/ml on average. TOOKAD-PDT of WISH-PC14 xenografts proved efficient by three parameters: tumor necrosis (2–3 days), tumor shrinkage and eradication (2–3 weeks), and a significant decline of serum PSA levels that could be detected within hours ($\geq$ 7 hours).

Monitoring the Early Response of Human WISH-PC14 Xenografts to TOOKAD-Based PDT by DW-MRI

Based on the successful eradication of human WISH-PC14 xenografts by the above PDT protocol, we further examined the response to treatment during the first 48 hours using DW-MRI. Following PDT of the tumor (Figure 2*A*, *PDT*), mean ADC values of untreated tumors (T) (time 0, 6.99 ± 0.64 × 10^{-4} SD mm^2/sec, n = 6) declined by ~25% (5.28 ± 0.74 × 10^{-4} mm^2/sec, P = .34 × 10^{-4}, n = 6) 7 hours

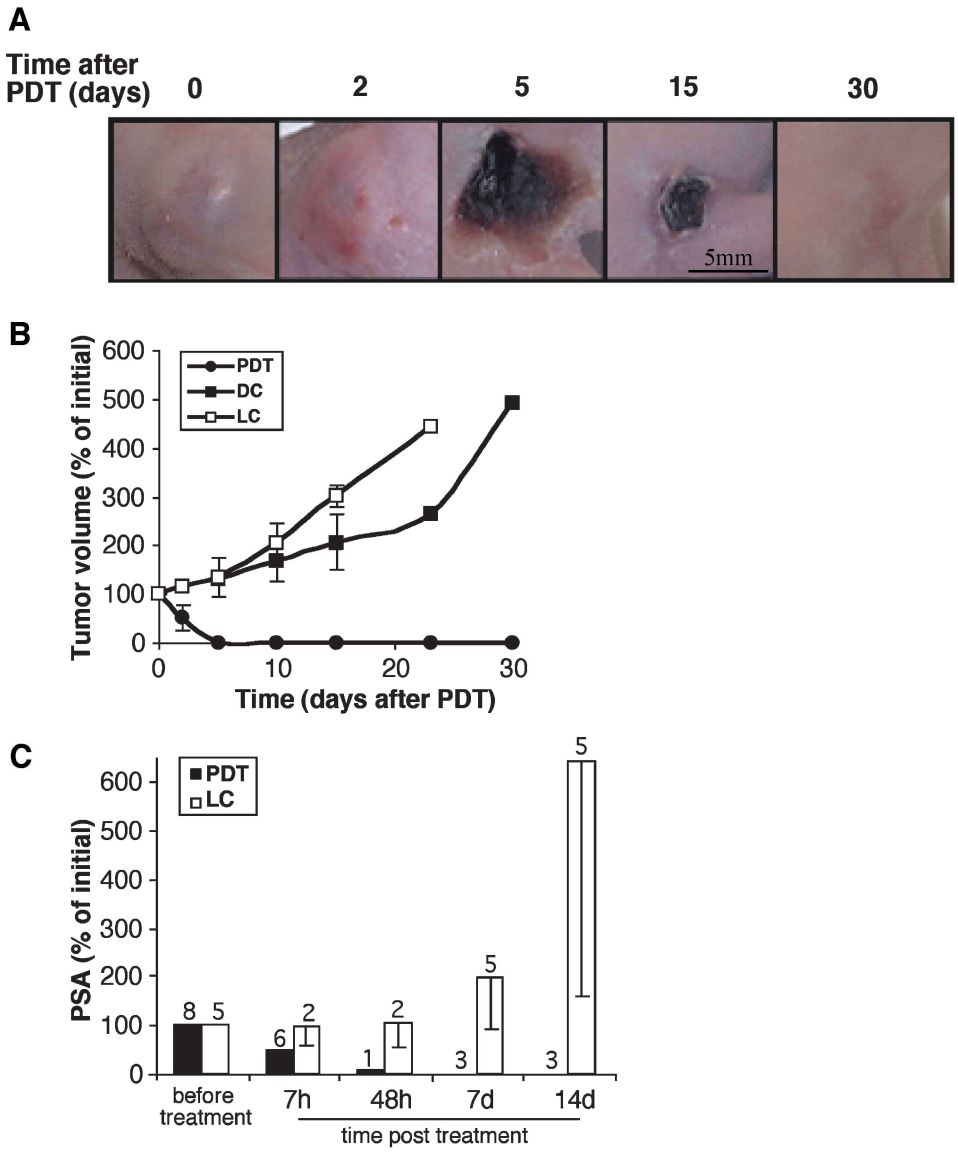

Figure 1. *The response of human WISH-PC14 xenografts to TOOKAD-based PDT. Direct examination of tumor response to TOOKAD-based PDT (10 mg/kg, 108 J/cm² for 10 minutes) before (0) and up to 30 days posttreatment (A). Tumor growth curves starting from day of treatment (day 0) are presented (B). The number of mice per PDT group: n = 9; light control (LC) and dark control (DC) groups: n = 4 each. Normalized (%) PSA levels in PDT and LC before and at indicated times after treatment are presented up to 14 days (C). Number of animals examined at each time point is indicated. Bars represent mean ± SD.*

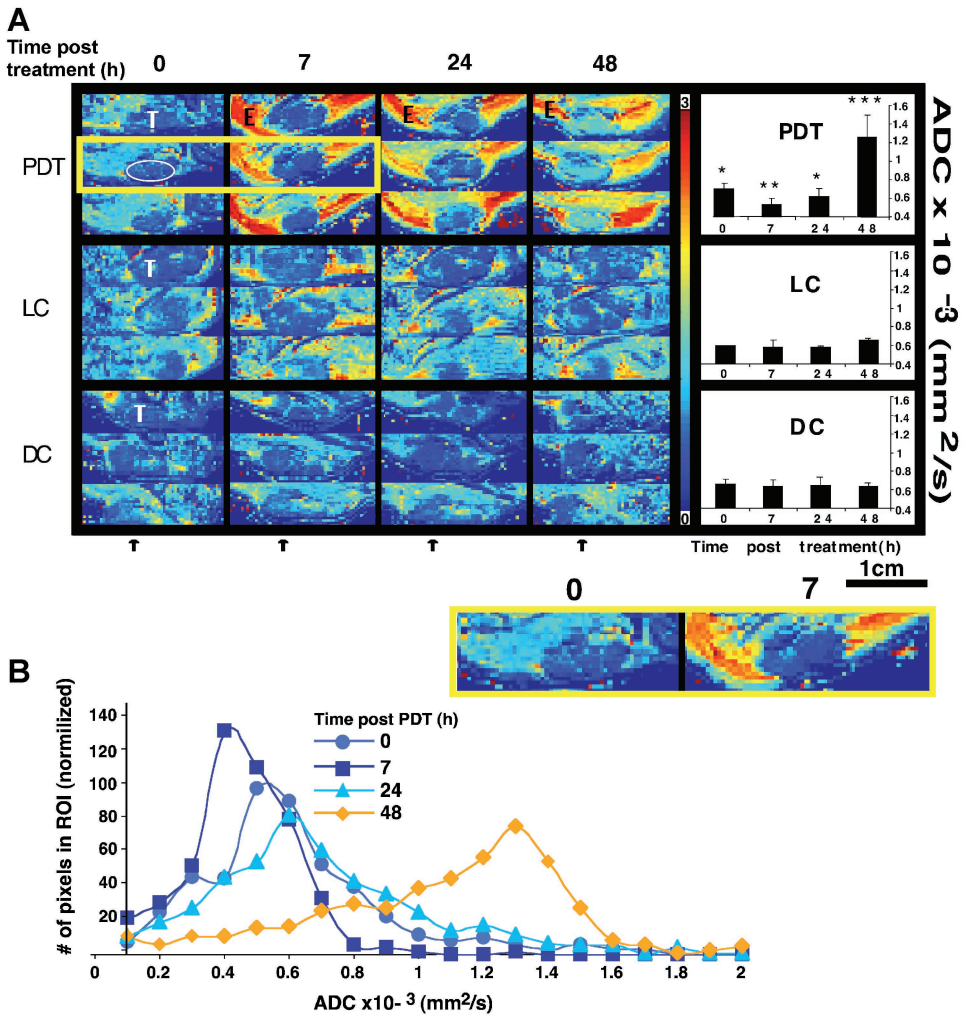

Figure 2. *Monitoring the early response of human WISH-PC14 xenografts to TOOKAD-based PDT by DW-MRI. Diffusion maps (A) of axial slices were generated, yielding ADC of each pixel of PDT-treated tumors (PDT) light control (LC) and dark control (DC) at indicated times before (0) and after treatment (7, 24, and 48 hours). For each time point, three consecutive axial slices are presented. Tumor (T), edema (E), and schematic illustration of ROI selection in tumor are indicated. Arrows indicate direction of illumination. Two enlarged representative slices before and 7 hours after treatment are also presented (lower box). DW images were evaluated by means of ROI measurements of the tumor area and ADC of tumors for PDT (n = 6), LC (n = 3), and DC (n = 3) was calculated and presented as bar graphs. Bars represent mean ± SD. Mean ADCs of each time point were subjected to paired two-tailed t-test, *, **, *** Significantly different from each other ($p < 0.005$). ADC histograms (B) were derived from ROIs of tumors after PDT (n = 3) and represent the distribution of ADC values at the times of measurement post-PDT. Results obtained in the representative tumor (A) are shown.*

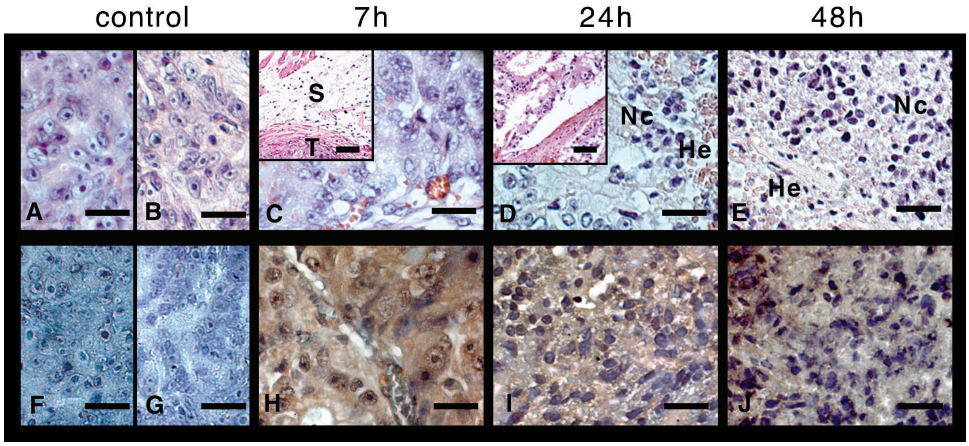

Figure 3. *Monitoring the response of human WISH-PC14 xenografts to TOOKAD-based PDT by histological and immunohistochemical examination. Tumors from light control (LC; A), dark control (DC; B), and 7, 24, and 48 hours post-PDT (C, D, and E, respectively) were fixed and stained with hematoxylin and eosin (n = 2 for each one presented in the figure). The same tumors from LC (F), DC (G), and 7, 24, and 48 hours post-PDT (H, I, and J, respectively) were also immunostained for LPO by anti–HNE antibodies. Scale bar = 50 μm.*

post-PDT. At 24 hours, mean ADC values increased (6.17 ± 1.00 × 10^{-4} mm^2/sec, P = .251, n = 6) to below the initial untreated levels. This increase is more apparent at the tumor rim. By 48 hours post-PDT, ADC was further increased (12.56 ± 2.39 × 10^{-4} mm^2/sec, P = .004, n = 6) up to 1.8-fold over values of untreated tumors, correlating with the development of hemorrhagic necrosis in the tumor (all t-tests presented above are relative to untreated).

In contrast to observations in the tumor, massive edema (E) associated with an increase in diffusion was observed in the surrounding illuminated tissue 7 hours after PDT. The enhanced contrast at the tumor boundaries emphasized tumor response to PDT. The changes in ADC in the tumor were all light- and sensitizer-dependent and no significant changes in ADC were observed in the light (n = 3) (Figure 2*A*, *LC*) or dark (n = 3) (Figure 2*A*, *DC*) controls. ADC histograms of PDT-treated tumors (n = 3) were generated and exhibited high pattern similarity. One such analysis (corresponding to ADC maps in Figure 2*A*, *PDT*) is presented (Figure 2*B*). Interestingly, this revealed that the biphasic change in tumor ADC values post-PDT was associated with respective narrowing (7 hours) and subsequent broadening (24 and 48 hours) of the ADC value distribution.

These results demonstrate for the first time that treatment of a human prostate xenograft with TOOKAD-PDT induces a unique and significant transient decline in ADC concomitant with a decline in PSA (Figure 1).

Monitoring the Response of Human WISH-PC14 Xenografts to TOOKAD-Based PDT by Histological and Immunohistochemical Examination

To validate the direct/clinical and DW-MRI observations, the response to treatment during the first 48 hours was histologically examined. In light (Figure 3*A*), dark (Figure 3*B*), and untreated (not shown) controls, live neoplastic cells were visible, exhibiting marked atypia. In addition, multifocal cyst formation and mild multifocal lymphoplasmacystic infiltration surrounding the mass were evident. At 7 hours post-PDT (Figure 3*C*), neoplastic cells were viable, although degenerative changes in the form of cytoplasmic vacuolation were observed. There was separation and smudging of dermal collagen consistent with edema (Figure 3*C*, *insert*; tumor [T] and traces consistent with edema in skin [S] are indicated). After 24 hours (Figure 3*D*), there were also multifocal hemorrhages (He) and necrotic/apoptotic cells (Nc) in the periphery of the tumor. The neoplastic cords were widely separated from each other, consistent with the presence of protein-poor edema (Figure 3*D*, *insert*). There was widespread necrosis of the overlying skin with relative sparing of the interfollicular epidermis. By 48 hours (Figure 3*E*), there was massive necrosis of the tumor with few peripheral hemorrhages and, as at 24 hours, widespread necrosis of the overlying skin.

Response to TOOKAD-PDT was also monitored by HNE staining for LPO (as a PDT response marker). Although negative HNE staining in all controls (Figure 3, *F* and *G*) indicated no traces of LPO, positive HNE staining (brown) throughout the tumor mass at 7, 24, and 48 hours post-PDT (Figure 3, *H–J*, respectively) indicated the presence of LPO. These results confirmed tumor damage progression and PDT-associated LPO in the illuminated tumor of a TOOKAD-treated mouse.

Monitoring the Response of Hepa-1 Spheroids to TOOKAD-Based PDT by DW-MRI

In order to examine the contribution of the tumor's nonvascular compartment to the observed change in PDT-induced ADC, we conducted a PDT experiment in multicellular spheroids simulating avascular tumors. As WISH-PC14 does not form spheroids *in vitro*, we used Hepa-1 cells to generate spheroids. The mean water ADC in an ROI containing the viable rim of untreated spheroids (Figure 4*A*) was 5.73 × 10^{-4} ± 0.23 SD mm^2/sec, whereas PDT-treated spheroids (Figure 4*B*) had a ~23% lower average ADC value of 4.42 × 10^{-4} ± 0.27 mm^2/sec (P = .003, two-tailed t-test). Data represent three independent experiments, with four to five spheroids per experimental group. Average ADC value of light, dark, and PI controls did not significantly differ from untreated control (data not shown). TOOKAD-induced photocytotoxicity was determined for all spheroids scanned by MRI using PI (prior to MRI examination). In control spheroids, there was no PI staining in the viable rim; however, PI staining was detected in cells located in the central hypoxic region. This region contains the necrotic core and the surrounding quiescent cells characterized by decreased pO_2 [21] (Figure 4*C*). After PDT, only spheroids that stained positively with PI in the former viable rim (FVR) were studied by MRI (Figure 4*D*). Consistent with PDT-treated tumors, histological sections of untreated spheroids did not stain for HNE in the viable rim (Figure 4*E*), whereas the rim region of PDT-treated spheroids stained positive for HNE (Figure 4*F*). Although there is some HNE staining in the hypoxic area, staining in the FVR appears only after PDT. It could therefore be concluded that the decline of ADC can also be induced *in vitro* in an avascular cell spheroid model.

Discussion

The major finding of this study is the unique temporal biphasic change in ADC observed in treated tumors within 24 hours after PDT with TOOKAD. This phenomenon is suggested as an early indicator of tumor response to this treatment. Furthermore, it is suggested that this transient response correlates with the desired treatment outcome (necrosis 48 hours post-PDT) culminating in tumor eradication. The PDT protocol used had an overall success rate of 74% using tumor necrosis as endpoint. The necrotic process developing over the first 24 to 48 hours (Figure 1*A*) led to flattening of the treated tumors by ~ day 5, yielding complete tissue remodeling by 30 days after PDT in 9 of 14 mice (Figure 1*B*). Temporal changes in blood supply to various tumor regions can result in heterogeneous distribution of the sensitizer and, hence, account for incomplete response to PDT. A significant reduction in PSA levels was already

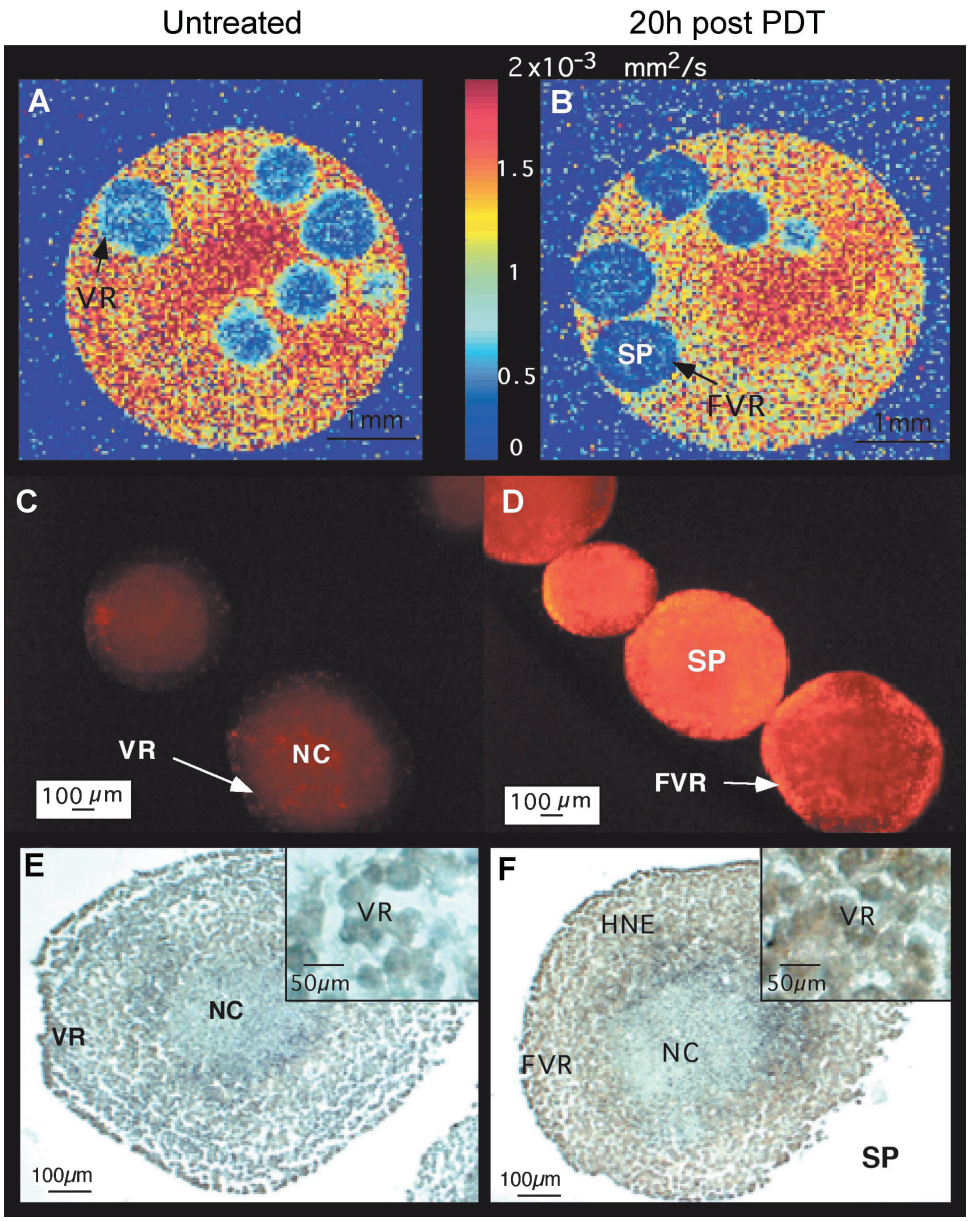

Figure 4. *Monitoring the response of Hepa-1 spheroids to TOOKAD-based PDT by DW-MRI. Hepa-1 spheroids were MRI-scanned before and 20 hours post-PDT. Diffusion maps of untreated controls (A) and PDT-treated spheroids (B) were generated. PI stainings of untreated controls (C) and PDT-treated spheroids (D) are shown. Anti–HNE stainings of untreated control (E) and PDT-treated (F) spheroid are shown. NC, necrotic core; VR, viable rim; FVR, former viable rim; SP, spheroid.*

apparent by 7 hours (Figure 1*C*), in agreement with other response parameters (Figure 2, *ADC*; Figure 3, *LPO*) and subsequent treatment outcome (Figure 1, *A* and *B*). These data support previous findings of our laboratory showing that a single treatment session of TOOKAD-PDT can successfully eradicate subcutaneous SCCP xenografts as well as orthotopic and intraosseous tumors in CD-1 nude mice [6]. PDT is known as a minimally invasive treatment that has profound and rapid effects on the treated tissue within minutes of illumination, inducing severe hemodynamic disturbances with consequent hypoxia [5,11,29]. It was therefore reasonable to correlate changes in tissue consistency developing within hours after treatment with the tracked changes in DW-MRI.

Conventional cancer treatment modalities like chemotherapy or radiotherapy require repetitive treatment sessions over periods of weeks to months. Consequently, response to treatment is slow and estimation of success by palpation or imaging (X-ray, ultrasonography, computed tomography, and MRI) as well as tumor markers may require substantial time elapse before detectable changes in size or contrast can be observed. In contrast, PDT practiced in ambulatory clinics or hospitals is short (approximately an hour) and estimation of response to treatment monitored within the day of treatment would be of great benefit. As demonstrated in this study, tumor necrosis by direct/clinical (Figure 1) and histological (Figure 3) parameters is consistent with an increase in ADC at the tumor rim (24 hours) covering the

entire tumor by 48 hours post-PDT (Figure 2, *A* and *B*). Of great importance is the observation that at 7 hours post-PDT, the decrease in tumor ADC (Figure 2, *A* and *B*) was coincidental with an increase in ADC in the surrounding normal tissue (due to edema) (Figure 2*A*). This concomitant inverse response observed on the tumor boundary enhances local MR contrast, demonstrating the differential and selective response of the two tissues to PDT. These PDT-induced changes correlate well with previous finding that showed tumor response by hemodynamic parameters [5] within minutes of illumination and by LPO within hours to days [6] (Figure 3). Minimal edema due to laser illumination is seen in light control (Figure 2*A*, *LC*) and is totally absent in dark control (Figure 2*A*, *DC*). Changes in ADC value distribution as shown in the histograms (Figure 2*B*) may represent an ADC signature of tumor response to TOOKAD-PDT, the basis of which has yet to be elucidated. We wish to state that although desirable in this study, animal imaging at a time interval shorter than 7 hours post-PDT was prohibited by the well being of the mice following anesthesia, but may be possible in humans.

The decline in ADC following TOOKAD-PDT is unique with respect to pattern and time of appearance compared with increase in ADC observed following most conventional therapies. In oncology and preclinical cancer models, early tumor response (characterized by high ADC) is usually referred to a minimum of 2 days after cytotoxic treatment, often prior to significant decrease in tumor size [30]. For example, an increase in ADC was described for the response of LnCaP human prostate adenocarcinoma xenografts to chemotherapy with docetaxel 2 days after treatment [13]. An increase in ADC of orthotopic rat brain 9L glioma tumors was also observed 2 days after 1,3-bis (2-chloroethyl)-1-nitrosourea (BCNU) treatment [31].

Increase in tumor ADC and necrotic response to therapy were shown to develop simultaneously. The histological characteristics of necrosis include increased ECS, reduced cellularity, and liberation of water from cells [19]. Increase in ADC is common for tumor response to cytotoxic treatments including a single report on ALA-PDT [32]. Decreased diffusivity has been described in normal brain tissues in association with acute cerebral ischemia [19] and following porphyrin-based Photofrin II-PDT in normal brain, where a biphasic temporal response pattern similar to the one described here was observed [33].

A biphasic temporal ADC response pattern was also observed after convection-enhanced Taxol delivery in brain tumor patients [34]. To the best of our knowledge, a decrease in ADC as a marker for early response to cytotoxic treatment of normal/tumorigenic tissue outside the brain has not been reported. ADC decrease is detected at later times (weeks) after therapy usually due to local regrowth [31] or fibrosis [35]. It is indeed possible that in the case of local tumor regrowth after TOOKAD-PDT, a decrease in ADC to pretreatment values may also be observed. Reduction in ADC of water in acute cerebral ischemia was originally attributed to a reduction of ECS volume fraction [19], whereas the decreased tumor ADC in our model at 7 hours was not associated with reduction of ECS (Figure 3*C*). However, the connection between ECS and ADC changes can only partially explain the observed changes in water diffusion associated with acute ischemia *in vivo* [19]. Decrease in water ADC could also result from alterations in intracellular compartmentalization, such as cytoplasmic vacuolation observed 7 hours post-PDT (Figure 3*C*), or changes in permeability of cell membranes to water and ions [36].

Ischemia and deoxygenation are also causes of tissue damage by Photofrin-PDT [37], bacteriochlorophyll serine-PDT [29], and TOOKAD-PDT [5]. Similar to bacteriochlorophyll-based PDT [5,7,11,29], the anti–tumor activity of combretastatin A4 prodrug was also antivascular and was shown to induce a significant decrease in perfusion and oxygenation of a murine sarcoma tumor immediately after treatment [38]. In the TOOKAD-PDT xenografts, ADC that was measured with relatively low *b* values (7–596 sec/mm^2) probably also reflects the antivascular effect that TOOKAD-PDT has on blood microcirculation in the tumor capillary network [39]. Indeed, a correlation between low oxygenation levels (caused by vascular occlusion) and low ADC in certain tumor regions was reported [40], but although combretastatin A4 induced a decline in oxygenation, it was not associated with a decrease in tumor ADC [38]. In contrast, TOOKAD-PDT suggests an association between a decline in oxygenation posttreatment [5] and a decrease in tumor ADC as reported here. We thus postulate that an additional common denominator between PDT and cerebral ischemia attributes to the decrease in ADC observed.

LPO is a response marker for PDT with TOOKAD (Figure 3) [5,6] and porphyrin derivatives [41], and has been described in the process of cerebral ischemia [42] but not in combretastatin action. Although LPO is initiated by photosensitized ROS, the dominant part of necrotic tumor damage in the case of TOOKAD-PDT spreads the tumor after illumination presumably by free radical chain reactions that are in progress by 7 hours after treatment (Figure 3*H*).

We suggest here that the decrease in ADC could result from endogenous generation of toxic LPO products derived from membrane lipid modifications. These may include cytotoxic aldehydes and peroxides that either cross-link or inactivate enzymes and transporters, leading to general metabolic arrest (e.g., depletion of ATP) [43], thereby blocking active ion and water transport. As a result, a transient decline in ADC may develop prior to cell lysis and necrosis, leading to water liberation and increase in ADC.

Because TOOKAD-PDT is an anti–vascular treatment where the target tumor cells are destroyed secondary to photodestruction of the tumor vasculature, it was important to establish the contribution of the nonvascular compartment of the tumor to the overall initial decrease in ADC. In order to examine this issue, we resorted to a cell spheroid as a model of an avascular tumor.

The experimental results obtained (Figure 4) seem to validate a decrease in ADC induced by TOOKAD-PDT in this model. Furthermore, these results support the dominant

role of the nonvascular compartment in the ADC decline during early stages of tumor response to PDT. These results are also consistent with the suggested role of LPO in the mechanism of ADC decline (Figure 4*F*). PI penetration into the cells of the spheroid FVR is passive yet PDT-dependent (Figure 4*D*). Thus, the observed changes in ADC are concomitant with an initial change in cell membrane permeability (permitting PI penetration) and do not involve hemodynamic or inflammatory processes. In the spheroid model, ADC was measured with relatively high *b* values (and other comparable parameters as previously reported) [22] and thus weighted heavier by the intracellular compartment. Nevertheless, if the decrease in ADC also represents a change in ADC of extracellular water, it is possible that LPO products departing from cell membranes into the ECS (still prior to necrosis) might increase tortuosity, thereby causing a transient decrease in ADC.

It should be noted that the ADC decrease in spheroids was determined only at 20 hours post-PDT, yet the principal observation and conclusion that PDT induces an initial rapid decline in ADC are essentially identical. The sustained low ADC in the *in vitro* model may relate to differences between models. In addition, the lack of decreased ADC at 20 hours *in vivo* differs from the *in vitro* model, suggesting a possible masking of the decline in ADC by a subsequent necrosis that results in increased ADC. This is either delayed *in vitro* or perhaps requires hemodynamic or inflammatory contributions that are absent in the spheroid model.

In summary, this study suggests that the rapid decline in ADC in human prostate adenocarcinoma xenografts can serve as an early response marker for successful TOOKAD-PDT apparent within 7 hours of treatment. TOOKAD-PDT of localized PC (currently in clinical trials) is enabled by short illumination using fiber optic light delivery immediately after intravenous injection of TOOKAD. It is important to provide the means for rapid assessment of tumor response and prediction of treatment outcome. The possible need for adjuvant or alternative treatment may thus be assessed within hours after treatment. Currently, the evaluation of treatment outcome of other minimally invasive anti–PC treatments (like brachytherapy) is based on PSA levels, dictating long time follow-up intervals as frequently observed when a more progressive disease is already attained. Although we observed a 50% drop in PSA levels as early as 7 hours after treatment in the human xenograft model, PSA levels in humans are not expected to change as fast, due to normal basal PSA secretion and a longer half life. In the case of other minimally invasive treatments (e.g., cryotherapy) that elicit rapid tumor response, the advantages of using MRI for analyzing the full extent of treatment during and after therapy are clear [44] and similar to those desired in PDT. The present study suggests the application of DW-MRI as a noninvasive rapid methodology for monitoring tumor response within a few hours after PDT. We believe that this technique may provide clinical advantages by allowing evaluation of tumor response on the day of treatment.

Acknowledgements

The authors thank Ori Brenner for pathological evaluations and Liora Shiftan for her help with the DW-MRI spheroid studies.

References

[1] Fuchs J, Weber S, and Kaufmann R (2000). Genotoxic potential of porphyrin type photosensitizers with particular emphasis on 5-aminolevulinic acid: implications for clinical photodynamic therapy. *Free Radic Biol Med* **28,** 537–548.

[2] Scherz A, Salomon Y, Scheer H, and Brandis A (1999). Palladium-substituted bacteriochlorophyll derivatives and use thereof. *International PCT Patent Application No. PCT/IL99/00673*.

[3] Schreiber S, Gross S, Brandis A, Harmelin A, Rosenbach-Belkin V, Scherz A, and Salomon Y (2002). Local photodynamic therapy (PDT) of rat C6 glioma xenografts with Pd-bacteriopheophorbide leads to decreased metastases and increase of animal cure compared with surgery. *Int J Cancer* **99,** 279–285.

[4] Dolmans DE, Fukumura D, and Jain RK (2003). Photodynamic therapy for cancer. *Nat Rev Cancer* **3,** 380–387.

[5] Gross S, Gilead A, Schertz A, Neeman M, and Salomon Y (2003). Monitoring photodynamic therapy of solid tumors online by BOLD contrast MRI. *Nat Med* **9,** 1327–1331.

[6] Koudinova NV, Pinthus JH, Brandis A, Brenner O, Bendel P, Ramon J, Eshhar Z, Scherz A, and Salomon Y (2003). Photodynamic therapy with Pd-Bacteriopheophorbide (TOOKAD): successful *in vivo* treatment of human prostatic small cell carcinoma xenografts. *Int J Cancer* **104,** 782–789.

[7] Preise D, Mazor O, Koudinova N, Liscovitch M, Scherz A, and Salomon A (2003). Bypass of tumor drug resistance by antivascular therapy. *Neoplasia* **5,** 475–480.

[8] Gross S, Gilead A, Mazor O, Brandis A, Schreiber S, Machluf Y, Neeman M, Scherz A, and Salomon Y (2003). Selective vascular and tumor responses to photodynamic therapy (PDT) with Pd bacteriopheophorbide (TOOKAD®): online and offline analyses *Proceedings of the 94th Annual Meeting of the American Association for Cancer Research (AACR).* **44**, p 121.

[9] Kato H, Patrice T, and Wilson B (1999). Photodynamic therapy. *Rev Contemp Pharmacother* **10,** 1–78.

[10] Macdonald IJ and Dougherty TJ (2001). Basic principles of photodynamic therapy. *J Porphyr Phthalocyanines* **5,** 105–129.

[11] Zilberstein J, Schreiber S, Bloemers MC, Bendel P, Neeman M, Schechtman E, Kohen F, Scherz A, and Salomon Y (2001). Antivascular treatment of solid melanoma tumors with bacteriochlorophyll-serine–based photodynamic therapy. *Photochem Photobiol* **73,** 257–266.

[12] Kelleher DK, Thews O, Rzeznik J, Scherz A, Salomon Y, and Vaupel P (1999). Water-filtered infrared-A radiation: a novel technique for localized hyperthermia in combination with bacteriochlorophyll-based photodynamic therapy. *Int J Hypertherm* **15,** 467–474.

[13] Jennings D, Hatton BN, Guo J, Galons JP, Trouard TP, Raghunand N, Marshall J, and Gillies RJ (2002). Early response of prostate carcinoma xenografts to docetaxel chemotherapy monitored with diffusion MRI. *Neoplasia* **4,** 255–262.

[14] Chen Q, Huang Z, Luck D, Beckers J, Brun PH, Wilson BC, Scherz A, Salomon Y, and Hetzel FW (2002). Preclinical studies in normal canine prostate of a novel palladium-bacteriopheophorbide (WST09) photosensitizer for photodynamic therapy of prostate cancers. *Photochem Photobiol* **76,** 438–445.

[15] Gertner MR, Bogaards A, Weersink RA, McCluskey SA, Haider MA, Yue CKK, Savard J, Simpson S, Brun PH, Cohen P, Scherz A, Salomon Y, Aprikian AG, Elhilali MM, Wilson BC, and Trachtenberg J (2003). Initial results of a Phase I/II trial of wst09-mediated photodynamic therapy (WST09-PDT) for recurrent prostate cancer following failed external beam radiation therapy (EBRT) *CapCure Scientific Retreat, Washington, DC*.

[16] He Z, Evelhoch JL, Mohammad RM, Adsay NV, Pettit GR, Vaitkevicius FH, and Sarkar FH (2000). Magnetic resonance imaging to measure therapeutic response using an orthotopic model of human pancreatic cancer. *Pancreas* **21,** 69–76.

[17] Poptani H, Duvvuri U, Miller CG, Mancuso A, Charagundla S, Fraser NW, Glickson JD, Leigh JS, and Reddy R (2001). T1rho imaging of murine brain tumors at 4 T. *Acad Radiol* **8,** 42–47.

[18] Padhani AR, MacVicar AD, Gapinski CJ, Dearnaley DP, Parker GJ, Suckling J, Leach MO, and Husband JE (2001). Effects of androgen

deprivation on prostatic morphology and vascular permeability evaluated with MR imaging. *Radiology* **218,** 365–374.
[19] Kauppinen RA (2002). Monitoring cytotoxic tumour treatment response by diffusion magnetic resonance imaging and proton spectroscopy. *NMR Biomed* **15,** 6–17.
[20] Song SK, Qu Z, Garabedian EM, Gordon JI, Milbrandt J, and Ackerman JJ (2002). Improved magnetic resonance imaging detection of prostate cancer in a transgenic mouse model. *Cancer Res* **62,** 1555–1558.
[21] Dubessy C, Merlin JM, Marchal C, and Guillemin F (2000). Spheroids in radiobiology and photodynamic therapy. *Crit Rev Oncol Hematol* **36,** 179–192.
[22] Smouha E and Neeman M (2001). Compartmentation of intracellular water in multicellular tumor spheroids: diffusion and relaxation NMR. *Magn Reson Med* **46,** 68–77.
[23] Neeman M, Jarrett KA, Sillerud LO, and Freyer JP (1991). Self-diffusion of water in multicellular spheroids measured by magnetic resonance microimaging. *Cancer Res* **51,** 4072–4079.
[24] Schertz A, Salomon Y, Scheer H, and Brandis A (1999). Palladium-substituted bacteriochlorophyll derivatives and use thereof. *International PC Patent Application No. PCT/IL99/00673*.
[25] Bar-Shira A, Pinthus JH, Rozovsky U, Goldstein M, Sellers WR, Yaron Y, Eshhar Z, and Orr-Urtreger A (2002). Multiple genes in human 20q13 chromosomal region are involved in an advanced prostate cancer xenograft. *Cancer Res* **62,** 6803–6807.
[26] Gleave ME, Hsieh JT, Wu HC, von Eschenbach AC, and Chung LW (1992). Serum prostate-specific antigen levels in mice bearing human prostate LNCaP tumors are determined by tumor volume and endocrine and growth factors. *Cancer Res* **52,** 1598–1605.
[27] Hankinson O, Adams GE, and Brindle KM (1979). Single-step selection of clones of a mouse hepatoma line deficient in aryl hydrocarbon hydroxylase. *Proc Natl Acad Sci USA* **76,** 373–376.
[28] Neeman M, Freyer JP, and Sillerud LO (1990). Pulsed-gradient spin-echo diffusion studies in NMR imaging. Effects of the imaging gradients on the determination of diffusion coefficient. *J Magn Reson* **90,** 303–312.
[29] Zilberstein J, Bromberg A, Frantz A, Rosenbach-Belkin V, Kritzmann A, Pfefermann R, Salomon Y, and Scherz A (1997). Light-dependent oxygen consumption in bacteriochlorophyll-serine–treated melanoma tumors: on-line determination using a tissue-inserted oxygen microsensor. *Photochem Photobiol* **65,** 1012–1019.
[30] Evelhoch JL, Gillies RJ, Karczmar GS, Koutcher JA, Maxwell RJ, Nalcioglu O, Raghunand N, Ronen SM, Ross BD, and Swartz HM (2000). Applications of magnetic resonance in model systems: cancer therapeutics. *Neoplasia* **2,** 152–165.
[31] Chenevert TL, Stegman LD, Taylor JM, Robertson PL, Greenberg HS, Rehemtulla A, and Ross BD (2000). Diffusion magnetic resonance imaging: an early surrogate marker of therapeutic efficacy in brain tumors. *J Natl Cancer Inst* **92,** 2029–2036.
[32] Roth Y, Orenstein A, Ruiz-Cabello J, Maier SE, Cohen J, and Mardor Y (2002). Pre-treatment and early monitoring of tumor response to therapy using diffusion-weighed MRI (DWMRI) *Proceedings of the 10th Scientific Meeting of the International Society for Magnetic Resonance in Medicine (ISMRM) P 2146*.
[33] Jiang Q, Knight RA, Chopp M, Helpern JA, Ordidge RJ, Qing ZX, and Hetzel FW (1991). ^{1}H magnetic resonance imaging of normal brain tissue response to photodynamic therapy. *Neurosurgery* **29,** 538–546.
[34] Mardor Y, Roth Y, Lidar Z, Jonas T, Pfeffer R, Maier SE, Faibel M, Nass D, Hadani M, Orenstein A, Cohen JS, and Ram Z (2001). Monitoring response to convection-enhanced Taxol delivery in brain tumor patients using diffusion-weighted magnetic resonance imaging. *Cancer Res* **61,** 4971–4973.
[35] Hein PA, Kremser C, Judmaier W, Griebel J, Pfeiffer KP, Kreczy A, Hug EB, Lukas P, and DeVries AF (2003). Diffusion-weighted magnetic resonance imaging for monitoring diffusion changes in rectal carcinoma during combined, preoperative chemoradiation: preliminary results of a prospective study. *Eur J Radiol* **45,** 214–222.
[36] Nicolay K, Braun KP, Graaf RA, Dijkhuizen RM, and Kruiskamp MJ (2001). Diffusion NMR spectroscopy. *NMR Biomed* **14,** 94–111.
[37] Fingar VH, Siegel KA, Wieman TJ, and Doak KW (1993). The effects of thromboxane inhibitors on the microvascular and tumor response to photodynamic therapy. *Photochem Photobiol* **58,** 393–399.
[38] Beauregard DA, Thelwall PE, Chaplin DJ, Hill SA, Adams GE, and Brindle KM (1998). Magnetic resonance imaging and spectroscopy of combretastatin A4 prodrug-induced disruption of tumour perfusion and energetic status. *Br J Cancer* **77,** 1761–1767.
[39] Le Bihan D, Breton E, Lallemand D, Aubin ML, Vignaud J, Laval-Jeantet M, Stegman LD, Taylor JM, Robertson PL, Greenberg HS, Rehemtulla A, and Ross BD (1988). Separation of diffusion and perfusion in intravoxel incoherent motion MR imaging. *Radiology* **168,** 497–505.
[40] Dunn JF, Ding S, O'Hara JA, Liu KJ, Rhodes E, Weaver JB, and Swartz HM (1995). The apparent diffusion constant measured by MRI correlates with pO_2 in a RIF-1 tumor. *Magn Reson Med* **34,** 515–519.
[41] Chatterjee SR, Murugesan S, Kamat JP, Shetty SJ, Srivastava TS, Noronha OP, Samuel AM, and Devasagayam TP (1997). Photodynamic effects induced by meso-tetrakis4-(carboxymethyleneoxy)phenyl porphyrin using rat hepatic microsomes as model membranes. *Arch Biochem Biophys* **339,** 242–249.
[42] Al Nita D, Nita V, Spulber S, Moldovan M, Popa DP, Zagrean AM, and Zagrean L (2001). Oxidative damage following cerebral ischemia depends on reperfusion—a biochemical study in rat. *J Cell Mol Med* **5,** 163–170.
[43] Kelleher DK, Thews O, Scherz A, Salomon Y, and Vaupel P (2003). Combined hyperthermia and chlorophyll-based photodynamic therapy: tumour growth and metabolic microenvironment. *Br J Cancer*. **89**, 2333–2339.
[44] Onik G (2001). Image-guided prostate cryosurgery: state of the art. *Cancer Control* **8,** 522–531.